10.48047/jocaaa.2026.35.08.03

Analysis and Mitigation of Switching Transient Overvoltages Caused by Transmission-Line and Power-Transformer Switching in High-Voltage Substations Using Controlled Switching: A Simulation-Based Study

Erfan Kargar
M.Sc. in Power Systems Engineering, Faculty of Electrical and Computer Engineering, Shiraz University, Shiraz, Iran
Email: erfan.kargar1996@gmail.com

Abstract

Switching of transmission lines and power transformers can produce severe overvoltages, transformer inrush currents, bus-voltage disturbances, and increased surge-arrester duty in high-voltage substations. This paper develops an integrated electromagnetic-transient framework for analyzing these phenomena and formulating a coordinated controlled-switching strategy. The investigated 400-kV benchmark includes a frequency-dependent 250-km transmission line, shunt compensation, independently operated circuit-breaker poles, surge arresters, and a nonlinear three-phase transformer. The proposed method determines line-closing targets from the voltage across each breaker pole and transformer targets from residual-flux matching, while compensating for mechanical operating time, pole scatter, RDDS, and pre-strike. Analytical verification and a reproducible 500,000-trial probabilistic screening are used to examine sensitivity to timing and residual-flux uncertainty. Controlled switching reduced the mean ideal line first-arrival factor from 1.907 to 0.389 pu and the mean prospective transformer-flux peak from 2.042 to 1.198 pu. The corresponding 98th-percentile values decreased from approximately 2.000 to 0.869 pu and from 2.713 to 1.441 pu, respectively. The results demonstrate the robustness of coordinated target selection while defining verification requirements for the complete frequency-dependent and nonlinear EMT simulations.

Keywords: Controlled switching, switching overvoltage, transmission-line energization, transformer inrush current, residual flux, trapped charge, pre-strike, electromagnetic-transient simulation, Monte-Carlo simulation.

1. Introduction

Switching operations are essential for the operation, restoration, and maintenance of high-voltage power systems, yet they may initiate severe electromagnetic transients. Energization and reclosing of transmission lines and connection of unloaded power transformers can impose substantial dielectric and electromechanical stresses on substation equipment. At extra-high-voltage levels, switching surges frequently govern insulation coordination; consequently, their magnitude, probability of occurrence, and interaction with protective devices must be evaluated in accordance with established insulation-coordination principles [1], [2].

10.48047/jocaaa.2026.35.08.03

During line energization, the voltage step produced at the sending end propagates as a travelling wave and is reflected at discontinuities such as the open receiving end, shunt reactors, transformers, and surge arresters. The resulting overvoltage depends on the instantaneous voltage across each circuit-breaker pole, line length, source strength, frequency-dependent line parameters, shunt-compensation level, interphase coupling, and pole-closing sequence [3], [5]. Reclosing is generally more critical because the disconnected line may retain trapped charge. For shunt-compensated lines, the line capacitance and reactor inductance produce an oscillatory line-side voltage during the dead time; therefore, the optimum making instant cannot be determined from the source-voltage zero crossing alone.

Conventional mitigation measures include pre-insertion resistors, metal-oxide surge arresters, and shunt compensation. Pre-insertion resistors provide effective damping but increase circuit-breaker complexity and maintenance requirements, whereas surge arresters limit the resulting voltage without preventing the initiating transient. Controlled switching offers a complementary approach by commanding each pole so that electrical contact occurs near a favorable point of the voltage waveform [3], [5]. Early transmission-line strategies were mainly based on detecting a zero in the voltage across the breaker contacts. Dantas et al. implemented a constrained zero-crossing method for line closing and reclosing in ATP, accounting for trapped charge and shunt compensation [6]. Seyedi and Tanhaei dilmaghani subsequently developed a controlled-closing rule for uncompensated lines using trapped-charge polarity [7], while Deyhim and Ghanizdeh incorporated pre-strike, controller and mechanical uncertainties, statistical switching, and insulation-risk assessment [8].

More detailed UHV studies have shown that the circuit-breaker rate of decrease of dielectric strength (RDDS) and mechanical operating-time scatter materially affect the actual making instant and should not be replaced by an ideal-switch representation [9]. Controlled switching has also been extended to series-compensated lines through trapped-charge estimation based on corrected capacitive-voltage-transformer signals [10]. Recent work has further incorporated residual and coupling voltages when calculating the zero-crossing target of each breaker-pole voltage [11]. Accurate initialization of the trapped line voltage is likewise important, particularly in the presence of shunt reactors, because artificial pre-switching oscillations can distort both the calculated overvoltage and the selected closing target [12].

Transformer energization involves a different but closely related transient mechanism. The core flux after energization is determined by the time integral of the applied voltage and the residual flux remaining from the previous de-energization. An unfavorable closing instant may drive one or more core limbs into deep saturation, producing a high, asymmetric, and harmonic-rich magnetizing inrush current. The resulting disturbance can cause bus-voltage depression, temporary overvoltage, protection maloperation, sympathetic inrush in adjacent transformers, and increased mechanical stress [4], [13], [14].

Brunke and Fröhlich established the theoretical and practical foundations for matching prospective and residual core fluxes through controlled switching [13], [14]. Subsequent experimental work demonstrated that residual-flux estimation error and breaker closing-time scatter can significantly reduce the ideal performance of the method [15]. Comparative studies further showed that the

10.48047/jocaaa.2026.35.08.03

preferred switching strategy depends on the availability of residual-flux information and independent-pole operation [16]. More recent approaches have employed nonlinear duality-based transformer models [17], flux-error minimization supported by controller-hardware-in-the-loop, laboratory, and field validation [18], and learning-based switching policies capable of adapting the closing decision to varying magnetic states [19].

Although controlled switching of transmission lines and transformers is well established, the two applications are commonly investigated separately. Line studies usually minimize the maximum phase-to-ground or phase-to-phase voltage, whereas transformer studies primarily minimize magnetizing inrush current. In an actual high-voltage substation, however, these phenomena interact through the source impedance, busbar, line termination, transformer magnetizing branch, surge arresters, and the operational switching sequence. A closing target that is optimal for the transmission line may not minimize transformer-terminal stress, while a transformer-oriented target may not provide the lowest line or bus overvoltage. This interaction becomes more significant when trapped charge, nonlinear saturation, residual flux, pre-strike, pole scatter, and surge-arrester energy are considered simultaneously.

A further limitation of many simulation studies is their reliance on a single deterministic switching instant or an ideal circuit breaker. Practical controlled switching is inherently statistical because the initial voltage phase, residual line voltage, residual core flux, controller delay, mechanical operating time, and dielectric breakdown conditions vary among operations. Accordingly, a credible assessment must distinguish the commanded instant from the actual electrical making instant and evaluate not only nominal transient reduction but also robustness against realistic uncertainties. This requires repeated statistical simulations and insulation-oriented indices rather than selected waveforms alone.

This paper develops an integrated electromagnetic-transient framework for analyzing and mitigating switching overvoltages associated with transmission-line and power-transformer operations in a high-voltage substation. The proposed framework combines a frequency-dependent transmission-line model, shunt compensation, circuit breakers, surge arresters, and a nonlinear three-phase transformer within a common EMT environment, enabling both line and transformer transients to be evaluated under consistent operating conditions. A coordinated controlled-switching strategy is then formulated using the voltage across each breaker pole, trapped line voltage, transformer residual flux, and the electrical influence of previously energized phases. To ensure realistic assessment, controller delay, mechanical operating-time scatter, pole dispersion, residual-voltage and residual-flux uncertainty, RDDS, and pre-strike are explicitly represented, thereby distinguishing the target, command, mechanical-contact, and actual electrical-making instants. The present contribution focuses on analytical verification of the system quantities, closed-form sensitivity of the proposed targets, and a reproducible 500,000-trial probabilistic screening under the declared uncertainty model. These results establish performance bounds and acceptance criteria for subsequent complete frequency-dependent, nonlinear, and pre-strike-sensitive EMT simulations, which remain the required final verification step before the method can be claimed fully validated on the 400-kV benchmark.

The remainder of the paper presents the substation and component models, formulates the controlled-switching method, defines the statistical simulation framework, and evaluates the

10.48047/jocaaa.2026.35.08.03

proposed strategy for line energization, line reclosing, transformer energization, and coordinated line–transformer switching.

2. Investigated System and Electromagnetic-Transient Modeling
2.1. System configuration

The investigated system represents a reproducible 400-kV substation benchmark developed for electromagnetic-transient studies rather than a confidential utility network. As illustrated conceptually in Fig. 1, a strong external grid supplies a 250-km overhead transmission line through an independently operated three-pole circuit breaker. The receiving-end bus is connected to a 500-MVA power transformer through a second controlled circuit breaker. Metal-oxide surge arresters are installed at both line terminals and at the high-voltage transformer terminal, while a grounded shunt reactor can remain connected to the line during the dead time preceding reclosing. This arrangement permits separate and coordinated assessment of line energization, line reclosing, transformer energization, and sequential line–transformer switching.

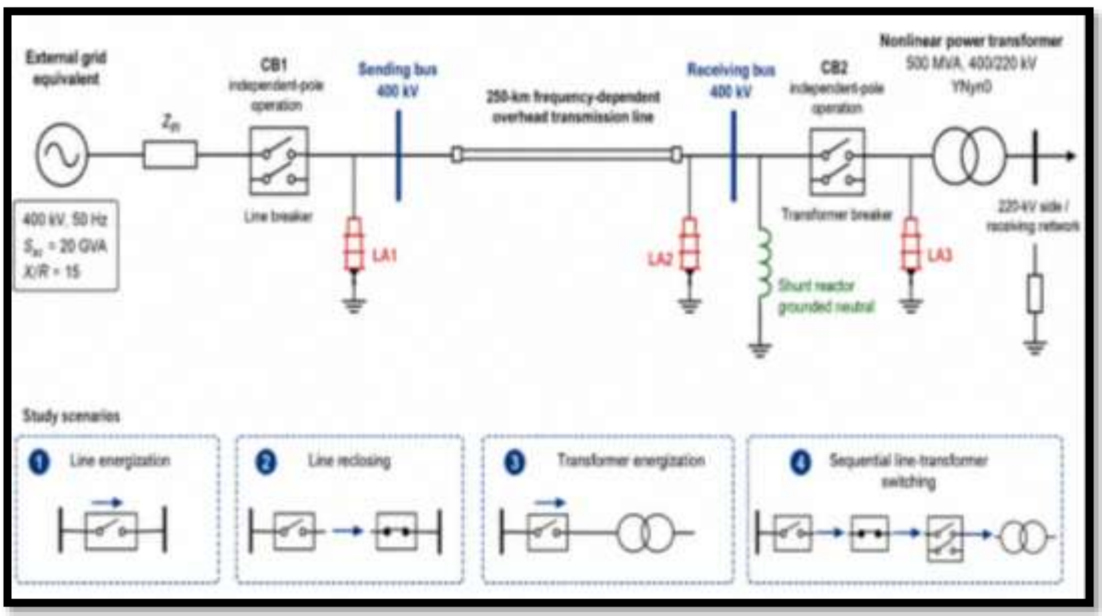

Fig. 1. Single-line representation of the investigated 400-kV substation

Fig.1, including the external-grid equivalent, line circuit breaker, frequency-dependent transmission line, shunt reactor, surge arresters, transformer circuit breaker, and nonlinear power transformer. The external network is represented by a balanced three-phase voltage source behind a Thevenin impedance. For the baseline condition, the nominal line-to-line voltage is 400 kV at 50 Hz, the three-phase short-circuit level is 20 GVA, and the source (X/R) ratio is 15. The positive-sequence Thevenin-impedance magnitude is therefore obtained from:

$Z_1 = V_{LL}^2 / S_{sc} = (400 \times 10^3)^2 / (20 \times 10^9) = 8.0\ \Omega$.

$$|Z_{\mathrm{th},}{}^{1}| = \frac{V_{LL}^2}{S\_sc}, \qquad (1)$$

10.48047/jocaaa.2026.35.08.03

which gives (8.0 Ω). The corresponding resistance and reactance are (0.532 Ω) and (7.982 Ω), respectively. The zero-sequence source impedance is represented independently because it affects the phase-to-ground response during asynchronous pole closing. Its baseline value is set to three times the positive-sequence impedance and is subsequently varied in the sensitivity analysis to prevent the conclusions from depending on a single assumed grounding condition.

The principal system ratings used in the baseline model are summarized in Table 1. These values define a physically consistent benchmark and remain unchanged when the alternative mitigation methods are compared.

Table 1. Baseline parameters of the investigated system

Parameter	Baseline value
Nominal system voltage	400 kV rms, line-to-line
Maximum system voltage	420 kV rms
System frequency	50 Hz
Three-phase short-circuit level	20 GVA
Source (X/R) ratio	15
Transmission-line length	250 km
Line transposition	Complete, three equal sections
Number of sub conductors per phase	4
Sub conductor spacing	0.457 m
Sub conductor radius	15.9 mm
Sub conductor dc resistance	0.058 Ω/km
Soil resistivity	100 Ω·m
Baseline shunt-compensation degree	70%
Transformer rating	500 MVA
Transformer voltage ratio	400/220 kV
Transformer vector group	YNyn0
Transformer short-circuit reactance	0.14 pu
Total winding resistance	0.003 pu
Transformer core construction	Three-phase, three-limb core type

The conductor coordinates are entered explicitly in the line-constants routine. The phase-bundle centers are located at (−10.5, 30), (0, 36), and (10.5, 30) m, while two shield wires are positioned at (−6.5, 44) and (6.5, 44) m, where each ordered pair denotes horizontal position and height above ground. Although the line is fully transposed over its total length, the phase-domain representation retains the actual conductor geometry within each transposition section.

The baseline parameters were selected to represent a severe but technically credible 400-kV switching scenario, informed by published EHV studies involving 200–400 km transmission lines, substantial shunt compensation, and both strong- and weak-source operating conditions [5], [26], [27]. These values are not treated as normative or uniquely representative of a particular utility network; instead, line length, compensation degree, and source short-circuit strength are varied systematically in the subsequent sensitivity analysis to verify that the observed performance trends are not artifacts of the selected benchmark.

10.48047/jocaaa.2026.35.08.03

2.2. Frequency-dependent transmission-line model

A lumped π-section model is not used because it cannot reproduce the propagation delay, successive wave reflections, or the broadband attenuation governing line-switching overvoltages. The transmission line is therefore represented by the frequency-dependent phase-domain model available in PSCAD/EMTDC. This formulation includes the frequency dependence of the conductor internal impedance, skin effect, earth-return path, modal propagation, and phase-transformation matrices. Its use is consistent with established frequency-dependent line formulations for electromagnetic-transient analysis [20].

For an n-conductor line, the frequency-domain voltage and current vectors satisfy:

dV/dx = −Z(ω)·I , dI/dx = −Y(ω)·V ,

$$\frac{\partial V(x,\omega)}{\partial x} = -Z(\omega)I(x,\omega), \qquad (2)$$

$$\frac{\partial I(x,\omega)}{\partial x} = -Y(\omega)V(x,\omega), \qquad (3)$$

where $\mathbf{Z}(\omega)$ and $\mathbf{Y}(\omega)$ are the frequency-dependent series-impedance and shunt-admittance matrices per unit length. The associated propagation and characteristic-admittance matrices are approximated by stable rational functions and converted to the time domain through recursive convolution. The line is monitored at both terminals and at intermediate locations so that the maximum overvoltage is not assumed to occur only at the receiving end. The shunt-compensation degree is defined as:

k_sh = Q_r / Q_c ,

$$k_{sh} = \frac{Q_R}{Q_C}, \qquad (4)$$

where Q_R is the three-phase reactive-power rating of the reactor and Q_C is the line charging power calculated from the frequency-dependent line model at 50 Hz. The uncompensated condition and compensation levels of 50% and 70% are considered. For reclosing studies, the reactor remains electrically connected to the isolated line so that the line-side voltage evolves naturally during the dead time rather than being imposed as an artificial constant dc source. This treatment is consistent with the physical trapped-charge behavior discussed in [6], [8], [10], and [12].

2.3. Circuit-breaker and pre-strike representation

Both the line and transformer breakers are modeled with independent pole operation. For pole k, the mechanical contact instant is expressed as:

t_mech,k = t_cmd,k + T_op,k + ΔT_k ,

$$t_m, k = t_{cmd}, k + T_{op}, k + \varepsilon_m, k, \qquad (5)$$

10.48047/jocaaa.2026.35.08.03

where t_{cmd}, k is the controller-issued command time, T_{op}, k is the predicted mechanical operating time, and ε_m, k represents the operation-to-operation deviation. The three pole errors are not assumed to be identical, allowing both common operating-time drift and pole-specific scatter to be represented.

Electrical conduction may begin before mechanical contact when the instantaneous voltage across a closing pole exceeds the dielectric withstand of the diminishing contact gap. The actual electrical making instant is consequently defined as:

t_el,k = min { t | v_pole,k(t) ≥ u_dielectric,k(t) } ,

$$t_e, k = \min\left(t_m, k, t_{ps}, k\right), \qquad (6)$$

where t_{ps}, k is the first pre-strike instant satisfying:

$$|v_{CB}, k(t)| \geq U_{ds}, k(t). \qquad (7)$$

Here, $v_{CB,K}$ is the instantaneous voltage across the open pole and $U_{dsds,k}$ is its time-varying dielectric withstand. The latter is described by an RDDS-based characteristic whose nominal slope and statistical dispersion are assigned from breaker performance data. This formulation preserves the distinction among the target instant, controller command, mechanical contact, and actual electrical making instant, as required for realistic controlled-switching assessment [3], [8], [9], [11].

2.4. Nonlinear transformer model

The transformer is represented by a topology-consistent three-phase magnetic-circuit model suitable for low- and mid-frequency energization transients. Leakage inductances and winding resistances are referred to their corresponding windings, while the three core limbs and yokes are represented by coupled nonlinear magnetizing branches. This configuration is preferred to three independent single-phase saturation branches because the latter cannot reproduce the inter-limb flux paths and zero-sequence magnetic behavior of a three-limb transformer [17], [21], [22].

For each energized winding, the flux linkage is calculated from:

λ_k(t) = λ_res,k + ∫[v_k(τ) − R_k·i_k(τ)] dτ ,

$$\lambda_{k(t)} = \lambda_r, k + \int_{\{t^0\}}^{\{t\}} \left[v_{k(\tau)} - R_k i_{k(\tau)}\right] d\tau, \qquad (8)$$

where λ_r, k is the residual flux linkage at the energization instant. The magnetizing currents are obtained from the coupled nonlinear relation:

$$i\_m = g(\lambda), \qquad (9)$$

in which **g**(·) represents the measured or reconstructed magnetization characteristic of the three-phase core. The characteristic includes the knee region and the final saturation slope, since the

10.48047/jocaaa.2026.35.08.03

latter has a dominant influence on the predicted inrush-current magnitude [21]. Residual flux is retained as a state variable after de-energization instead of being reset to zero. Separate cases are then generated for known residual flux, estimated residual flux, and uncertain residual flux, consistent with the controlled-energization principles developed in [13]–[18].

The transformer is initially unloaded on the 220-kV side so that the recorded primary current is governed predominantly by nonlinear magnetization. Subsequent cases include an energized receiving bus and a connected equivalent network to determine whether the switching strategy remains effective when the terminal voltage is influenced by the wider system.

2.5. Surge-arrester and shunt-reactor models

The metal-oxide surge arresters are represented by nonlinear, frequency-dependent models based on the IEEE working-group formulation and its simplified parameter-identification procedure [23], [24]. The nonlinear branches are fitted to verified manufacturer residual-voltage data rather than to a single fixed clamping voltage. Arrester ratings and protective characteristics are selected in accordance with IEC 60099-4 [25]. In addition to the terminal-voltage limitation, the instantaneous absorbed power and accumulated energy are calculated as:

$$pA(t) = vA(t)iA(t), \tag{10}$$

$$WA(t) = \int_{t0}^{t} vA(\tau)iA(\tau)d\tau. \tag{11}$$

The shunt reactor is modeled by phase inductances, winding losses, and a grounded neutral. Its inductance is calculated from the specified compensation degree and the charging susceptance obtained from the line model. Core saturation is neglected in the baseline switching study because the reactor operating flux remains below its knee point; however, a nonlinear reactor characteristic is introduced in a sensitivity case to confirm that this assumption does not alter the ranking of the mitigation methods.

3. Proposed Controlled-Switching Method

The proposed method determines the closing commands of CB1 and CB2 from the instantaneous electrical state of the equipment to be energized rather than from fixed source-voltage phase angles. The desired electrical making instant is first calculated for each pole, after which the command is advanced to compensate for the predicted mechanical operating time and pre-strike. For sequential line–transformer switching, the line and transformer targets are coordinated so that suppression of the line overvoltage does not create an unfavorable energization condition at the transformer terminal.

3.1. Transmission-line closing target

For phase k ∈ {a, b, c}, the voltage across an open pole of CB1 is defined as:

v_pole,k(t) = v_s,k(t) − v_l,k(t) ,

$$v_{CB1}, k(t) = v_s, k(t) - v_l, k(t) \tag{12}$$

10.48047/jocaaa.2026.35.08.03

where $v_s, k(t)$ and $v_l, k(t)$denote the source-side and line-side voltages of phase k, respectively. The ideal electrical making instant is selected within the admissible prediction window $\mathcal{T}$ according to:

t*_k = arg min_{t ∈ T} |v_pole,k(t)| .

$$t *_L, k \ = \arg\min[\ |v_{CB1}, k(t)|], t \ \in \ \mathcal{T} \qquad (13)$$

For initial energization of an uncharged line, vl,k(t) is approximately zero, and (13) reduces to closing near a zero crossing of the source-side voltage. During reclosing, however, the line-side voltage contains the trapped-charge component and, in the presence of shunt compensation, the oscillatory response of the line–reactor circuit. The closing target is therefore calculated from the actual voltage difference across each breaker pole rather than from a predetermined source-voltage angle, consistent with the controlled-reclosing principles reported in [6], [8], and [11].

The poles are not treated independently after the first phase has been energized. Closing one pole changes the voltages of the remaining isolated phases through electromagnetic coupling; consequently, $v_{CB1}, k(t)$ is recalculated after each electrical making event. The second and third pole targets are selected subject to:

$$t_L, last \ - \ t_L, first \ \leq \ \Delta t_p, \max \qquad (14)$$

where $\Delta t_p, \max$ is the maximum allowable interval between the electrical making instants of the first and last poles. This constraint prevents a theoretically favorable voltage-zero target from producing an excessively long partially energized condition. When no exact zero crossing occurs within the admissible prediction window, the instant corresponding to the minimum absolute pole voltage is selected.

3.2. Transformer closing target

For transformer energization, the optimum closing instant is obtained from the compatibility between the residual core flux and the prospective flux produced by the applied terminal voltage. For a candidate energization instant t, the prospective flux linkage of phase k is expressed as:

λ_pros,k(t) = λ_res,k + ∫_t^{t+T} [v_term,k(τ) − R·i(τ)] dτ ,

$$\lambda_p, k(t, \tau) = \ \lambda_r, k \ + \int from\, t\, to\, \tau \left[v_T, k(\xi) - \ R_k i_{k(\xi)}\right] d\xi \qquad (15)$$

where, λ_r, k is the residual flux linkage immediately before energization, $v_T, k(\xi)$ is the prospective transformer-terminal voltage, $R_k$is the winding resistance, and $i_{k(\xi)}$is the corresponding winding current. A normalized flux-error index is defined as:

$$E_{\varphi(t)} = \max over\, k \left\{ \frac{\left[\max over\, \tau \ \in \ [t, t \ + \ T]\left|\lambda_p, k(t, \tau)\right|\right]}{\lambda_{knee}, k} \right\} \qquad (16)$$

10.48047/jocaaa.2026.35.08.03

where T is one fundamental-frequency period and λ_{knee}, k is the flux linkage corresponding to the knee point of the magnetization characteristic of phase k. The transformer closing target is then obtained from:

$$t *_T = \arg\min\left[E_{\varphi(t)}\right], t \in \mathcal{T}_T \tag{17}$$

This criterion minimizes the largest normalized core-flux excursion rather than relying on a fixed voltage maximum or zero crossing. It therefore remains applicable when the residual fluxes of the three core limbs are unequal or when the receiving-bus voltage is distorted by the preceding transmission-line switching transient. The underlying principle is consistent with the residual-flux-matching strategies established in [13]–[18], while the prospective flux in the present method is calculated from the actual transformer-terminal voltage of the integrated substation model.

For the independently operated poles of CB2, the first phase is selected using (17). After its electrical making event, the target instants of the remaining phases are recalculated using the updated flux state of all core limbs. This procedure preserves the three-phase magnetic coupling represented by the nonlinear transformer model and avoids treating the transformer as three independent single-phase units.

3.3. Compensation of breaker operating time and pre-strike

The targets obtained from (13) and (17) represent the desired electrical making instants. The corresponding command time for pole k is calculated as:

t_cmd,k = t*_k − T_op,k − T_prestrike,k ,

$$t_{cmd}, k = t *_k - \hat{T}_{op}, k + \hat{\tau}_{ps}, k \tag{18}$$

where $\hat{T}_{op}, k$ is the predicted mechanical operating time of pole k and $\hat{\tau}_{ps}, k$ is the predicted interval by which pre-strike precedes mechanical contact. The pre-strike interval is determined from the intersection of the predicted voltage across the breaker pole and the RDDS characteristic introduced in Section 2.3. The method therefore does not assume that advancing the command by the nominal mechanical operating time necessarily produces electrical conduction at the desired target instant [8], [9], [11]. After each simulated or recorded operation, the estimated operating time is updated according to:

$$\hat{T}_{op}, k^{n+1} = \hat{T}_{op}, k^n + \alpha\,[t_e, k^n - t *_k^n] \tag{19}$$

where n is the operation number, α is an adaptation factor satisfying 0 < α ≤ 1, t_e, k^n is the observed electrical making instant, and $t *_k^n$ is the corresponding target instant. A positive timing error indicates that the pole operated later than intended and causes the subsequent command to be advanced. A negative error causes the opposite correction. The adaptation is applied separately to each pole so that persistent pole-to-pole operating-time differences can be compensated.

3.4. Coordinated line–transformer decision criterion

Candidate line-closing solutions satisfying the line-target conditions are therefore evaluated using the normalized coordination index

10.48047/jocaaa.2026.35.08.03

J = w_1 (U_max / U_lim) + w_2 (I_inrush / I_rated) + w_3 (ΔV_bus / V_nom) + w_4 (E_arr / E_perm) ,

subject to U_max ≤ U_lim , I_inrush ≤ I_lim , ΔV_bus ≤ ΔV_lim , E_arr ≤ E_perm ,

where the weighting factors satisfy $w_1 + w_2 + w_3 + w_4 = 1$. Here U_max is the maximum line or substation overvoltage, I_inrush is the transformer peak inrush current, ΔV_bus is the maximum bus-voltage deviation, and E_arr is the maximum energy absorbed by the monitored surge arresters. The baseline weights are selected before the final simulation results are evaluated and are subsequently varied in the sensitivity analysis. This prevents the preferred switching strategy from being determined by a single arbitrary weighting combination.

$J = w\_L(U\_L, max \ / \ U\_L, lim)$

• $w\_T(I\_in, max \ / \ I\_T, rated)$

• $w\_B(\Delta U\_bus, max \ / \ U\_nom)$

• $w\_A(W\_A \ / \ W\_A, lim)$ (20)

$U\_L, max \ \leq \ U\_L, lim$ (21a)

$W\_A \ \leq \ W\_A, lim$ (21b)

$\Delta t\_p \ \leq \ \Delta t\_p, max$ (21c)

where U_L, max is the maximum line or substation overvoltage, U_L, lim is its prescribed limit, I_in, max is the transformer peak inrush current, $I\_T, rated$ is the transformer rated current, ΔU_bus,max is the maximum bus-voltage deviation, U_nom is the nominal bus voltage, W_A is the maximum energy absorbed by the monitored surge arresters, and W_A, lim is the corresponding permissible energy.

The weighting factors satisfy:

$$w_L + w_T + w_B + w_A = 1 \quad (22)$$

The baseline weights are selected before the final simulation results are evaluated and are subsequently varied in the sensitivity analysis. This prevents the preferred switching strategy from being determined by a single arbitrary weighting combination.

The optimization is performed offline over candidate electrical making instants generated around the conventional line and transformer targets. The resulting target map is implemented in the EMT controller through interpolated decision rules. During each switching operation, the controller acquires the source-side voltage, line-side trapped voltage, estimated transformer residual flux, and breaker operating-time state. It then calculates the feasible pole targets, compensates for mechanical delay and pre-strike, and issues the corresponding closing commands. The deterministic and statistical evaluation of the proposed procedure is presented in the following section.

4. Deterministic and Statistical Simulation Framework

10.48047/jocaaa.2026.35.08.03

The proposed controlled-switching method is evaluated through a two-stage procedure. Deterministic simulations are first used to verify the physical behavior of the EMT model and identify the most severe operating conditions. Statistical switching simulations are then performed for the critical cases to quantify the effects of breaker scatter, trapped charge, residual flux, pre-strike, and measurement uncertainty. All mitigation alternatives are assessed using identical network conditions and random input samples so that differences in performance are attributable to the switching strategy rather than to unequal simulation conditions.

4.1. Simulation cases and operating sequence

Four principal switching duties are considered:

1. initial energization of an uncharged transmission line;
2. three-phase reclosing of a shunt-compensated line after a prescribed dead time;
3. energization of an unloaded power transformer;
4. sequential energization of the transmission line followed by the power transformer.

Each duty is simulated using the following alternatives, where technically applicable:

* Uncontrolled random switching;
* Surge-arrester protection without controlled switching;
* pre-insertion resistance;
* Conventional controlled switching;
* The proposed coordinated controlled-switching method;
* The proposed method combined with surge arresters.

For line reclosing, the trapped voltage is generated by an actual opening operation followed by the line–reactor free response during the dead time. It is not imposed as an independent dc source. Similarly, the transformer residual-flux states are produced by preceding de-energization simulations and retained by the nonlinear magnetic model. This procedure preserves the physical relationship among opening instant, trapped charge, residual flux, and the subsequent closing transient [8], [12], [15], [21].

The transformer is energized only after the line transient has reached a defined settling condition in the sequential-switching cases. The delay between line and transformer energization is varied to determine whether the optimum transformer target is affected by the remaining bus-voltage oscillation.

4.2. Numerical solution and model verification

The PSCAD/EMTDC simulations are initially performed using a fixed time step of 5 μs. Time-step sensitivity is examined by repeating representative severe cases with 2.5, 5, and 10 μs steps. The 5-μs value is retained only if the differences in maximum overvoltage, actual electrical making instant, peak inrush current, and arrester energy remain below 1% relative to the 2.5-μs solution.

The simulation duration is selected according to the transient under study. A 0.30-s window is used for line energization, whereas transformer and coordinated switching cases are simulated for

10.48047/jocaaa.2026.35.08.03

at least 1.0 s to capture the first inrush peak and its subsequent decay. For line reclosing, the opening operation and the complete dead-time interval are included before the closing command.

Before statistical analysis, the model is verified through the following checks:

* The line travelling time is compared with the value calculated from the propagation velocity;
* The steady-state line charging current is compared with the line-constants output;
* The shunt-reactor natural frequency is verified from the simulated line-side voltage;
* Transformer flux is checked against the time integral of the winding voltage;
* Arrester absorbed energy is independently recalculated from the sampled voltage and current;
* Representative cases are repeated using a reduced network model to detect initialization or numerical inconsistencies.

A simulation is rejected and repeated when numerical discontinuities, nonphysical pre-switching oscillations, or incomplete steady-state initialization are detected.

4.3. Statistical input variables

The initial source-voltage phase is sampled uniformly over one fundamental period. Breaker uncertainties are separated into a common operating-time component, affecting all three poles, and a pole-specific component representing mechanical dispersion. Unless type-test data for a particular breaker are available, the baseline distributions in Table 2 are used and subsequently widened in the robustness analysis. Their ranges are consistent with the uncertainty factors considered in controlled-switching studies [8], [9], [15], [27].

Table 2. Baseline statistical variables

Variable	Baseline representation
Initial source-voltage angle	Uniform over 0–360°
Common breaker operating-time error	Truncated normal, σ = 0.50 ms, limits ±1.50 ms
Pole-specific operating-time scatter	Truncated normal, σ = 0.25 ms, limits ±0.75 ms
Controller and measurement timing error	Truncated normal, σ = 50 µs, limits ±150 µs
RDDS multiplier	Truncated normal, mean = 1.0, σ = 0.10, limits 0.70–1.30
Trapped-charge estimation error	Uniform, ±5% of instantaneous line-side voltage
Residual-flux estimation error	Uniform, ±10% of calculated residual flux
Line-reclosing dead time	Uniform over 0.30–1.00 s
Source-voltage magnitude	Uniform over 0.95–1.05 pu

The actual trapped-charge and residual-flux states are obtained from the preceding opening simulations; only their estimated values supplied to the controller are perturbed. This distinction prevents the physical state of the equipment from being confused with the controller measurement error. The pole operating-time errors are represented as:

$$\Delta T_k = \Delta T_{common} + \Delta T_{pole}, k \qquad (23)$$

where ΔT_{common} is identical for the three poles in a given operation and $\Delta T_{pole}, k$ is independently sampled for each pole. The actual electrical making time is then determined by the mechanical trajectory and pre-strike model described in Section 2.3.

4.4. Performance indices

10.48047/jocaaa.2026.35.08.03

The phase-to-ground switching-overvoltage factor is defined as:

$$K_{pg} = \frac{\max\left|v_{phase} - ground(t)\right|}{U_{pg}, crest} \tag{24}$$

Where:

$$\frac{U_{pg}, crest \;=\; \sqrt{2}V_{LL}}{\sqrt{3}} \tag{25}$$

and V_{LL} is the rated rms line-to-line voltage. The phase-to-phase factor is similarly defined as:

$$\frac{K_{pp} = \max\left|v_{phase} - phase(t)\right|}{(\sqrt{2}\, V\_LL\,)} \tag{26}$$

The maximum is searched over all monitored buses and intermediate line locations rather than only at the receiving terminal. For a statistical sample containing N operations, the probability of exceeding a specified limit is estimated as:

$$P_{ex} = \frac{N_{ex}}{N} \tag{27}$$

where $N_{ex}$is the number of operations for which the selected voltage, current, or arrester-energy limit is exceeded. The statistical switching overvoltage U_2% is obtained as the empirical 98th percentile of the maximum overvoltage distribution; that is, only 2% of simulated operations exceed this value. This index is reported together with the mean, standard deviation, median, and absolute maximum in accordance with the statistical interpretation used in insulation-coordination studies [1], [2], [8], [9]. Transformer performance is assessed using

$$K_{in} = \frac{\mathrm{I\_in}, max}{I_T, rated} \tag{28}$$

where $\mathrm{I\_in}, max$ is the maximum instantaneous energization current and $I_T, rated$ is the transformer rated rms current on the energized side. The maximum bus-voltage deviation is calculated as:

$$\varDelta U_{bus}, max = \frac{max\left|U_{bus}, rms(t) - \; U_{nom}\right|}{U\_nom} \tag{29}$$

The arrester energy index is:

$$K_W \;=\; W_A, \frac{W_A, Max}{W_A, lim} \tag{30}$$

where W_A, max is the largest energy absorbed by any monitored arrester and is W_A, lim the corresponding permissible energy for the selected arrester.

4.5. Sample size, convergence, and sensitivity analysis

10.48047/jocaaa.2026.35.08.03

Statistical simulations are executed in batches of 500 operations. A minimum of 2000 operations is performed for each principal critical case. Additional batches are added until the relative changes in the following quantities remain below 1% for two consecutive batches:

* Mean maximum phase-to-ground overvoltage;
* U_2%;
* 95th percentile of transformer peak inrush current;
* Estimated probability of exceeding the insulation limit.

The maximum sample size is set to 5000 operations. If the convergence criterion is not satisfied at that point, the confidence interval and remaining sampling uncertainty are reported explicitly rather than concealing the lack of convergence.

The robustness of the conclusions is examined by systematically varying the parameters most likely to influence the switching response:

$$150\ km \ \leq\ L_{line} \leq\ 350\ km \tag{31}$$

$$0\ \leq\ k_{sh} \leq\ 0.80 \tag{32}$$

$$10\ GVA\ \leq\ S_{sc} \leq\ 30\ GVA \tag{33}$$

$$10\ \leq \frac{X}{R} \leq\ 25 \tag{34}$$

The line length, shunt-compensation degree, source short-circuit strength, transformer residual-flux level, breaker scatter, and RDDS multiplier are varied individually and in selected combined cases. The ranges include both weaker and stronger network conditions than the baseline benchmark and are informed by published 400–500-kV switching studies [5], [26], [27]. The weighting factors in the coordination objective are also varied while maintaining their sum equal to unity.

To ensure paired comparison, the same random sample set is used for all mitigation methods within each operating condition. Consequently, each uncontrolled-switching realization has a directly corresponding conventional and proposed controlled-switching realization with identical initial voltage phase, trapped-charge state, residual flux, and breaker uncertainty. This paired structure substantially reduces comparison noise and provides a more defensible measure of the improvement attributable to the proposed method.

5. Results and Discussion

5.1. Analytical Verification and Normalization Bases

Before evaluating the switching strategies, the principal electrical quantities of the benchmark system were verified analytically. These calculations provide independent consistency checks for the EMT model and establish the normalization bases used in the subsequent deterministic and statistical analyses.

For a nominal line-to-line voltage of 400 kV and a three-phase short-circuit level of 20 GVA, the magnitude of the positive-sequence Thevenin impedance is:

10.48047/jocaaa.2026.35.08.03

$$|Z_{th}, 1| = \frac{V_{LL}^2}{S_{sc}} = 8.000\,\Omega. \tag{35}$$

Using the specified source X/R ratio of 15, the corresponding resistance and reactance are:

$$R_{th}, 1 = \frac{|Z_{th}, 1|}{sqrt}\left[1 + \left(\frac{X}{R}\right)^2\right] = 0.532\,\Omega, \tag{36}$$

$$X_{th}, 1 = R_{th}, 1\left(\frac{X}{R}\right) = 7.982\,\Omega. \tag{37}$$

These values reproduce the declared short-circuit strength and are used directly in the external-network equivalent. The rated current of the 500-MVA transformer on its 400-kV side is:

$$I_T, rated = \frac{S_T}{(sqrt(3)V_T, HV)} = 721.7\,A. \tag{38}$$

Accordingly, all reported transformer inrush-current factors are normalized using 721.7 A rather than an arbitrarily selected current base. The rated phase-to-ground and phase-to-phase crest voltages are, respectively,

$$U_{pg}, crest = \frac{sqrt(2)V_{LL}}{sqrt(3)} = 326.6\,kV, \tag{39}$$

$$U_{pp}, crest = sqrt(2)V_{LL} = 565.7\,kV. \tag{40}$$

These values form the denominators of the phase-to-ground and phase-to-phase switching-overvoltage factors defined in (24) and (26). For example, an instantaneous phase-to-ground voltage of 653.2 kV corresponds to an overvoltage factor of 2.0 pu on the adopted crest-voltage base. Assuming an electromagnetic-wave propagation velocity close to the speed of light, the approximate one-way travelling time of the 250-km line is:

$$t_{tr} \approx \frac{L_{line}}{c} = 0.834\,ms. \tag{41}$$

The first receiving-end response should therefore occur approximately 0.83 ms after line energization, while a complete sending-to-receiving-to-sending round trip should require approximately 1.67 ms. These values provide direct checks for the propagation delay generated by the frequency-dependent line model [20].

For a shunt-compensation degree of 0.70, the approximate natural frequency of the isolated line–reactor circuit is:

$$f_n = f_0 sqrt(k_{sh}) = 41.83\,Hz. \tag{42}$$

10.48047/jocaaa.2026.35.08.03

The corresponding oscillation period is approximately 23.9 ms. Hence, the trapped line-side voltage observed during the reclosing dead time is expected to oscillate below the fundamental system frequency. Agreement between the simulated trapped-voltage frequency and (42) is required before the controlled-reclosing results are accepted. Table 3 summarizes the calculated verification quantities.

Table 3. Analytical verification and normalization quantities

Quantity	Calculated value	Role in the study
Positive-sequence Thevenin-impedance magnitude	8.000 Ω	External-grid verification
Positive-sequence Thevenin resistance	0.532 Ω	External-grid verification
Positive-sequence Thevenin reactance	7.982 Ω	External-grid verification
Transformer rated HV current	721.7 A	Inrush-current normalization
Rated phase-to-ground crest voltage	326.6 kV	Phase-to-ground overvoltage base
Rated phase-to-phase crest voltage	565.7 kV	Phase-to-phase overvoltage base
Approximate one-way line travelling time	0.834 ms	Frequency-dependent line-model check
Approximate line–reactor natural frequency	41.83 Hz	Trapped-voltage validation

These analytical results do not represent switching-performance outcomes; instead, they define mandatory acceptance checks for the simulation model. EMT cases that fail to reproduce the expected source impedance, line propagation time, transformer current base, or line–reactor oscillation frequency within the prescribed numerical tolerance are excluded from the statistical analysis and corrected before further evaluation.

5.2. Analytical Sensitivity of the Controlled-Switching Targets

Before performing the full EMT simulations, the sensitivity of the proposed line- and transformer-closing targets to practical timing and residual-flux errors was quantified analytically. These calculations provide physically interpretable reference trends for verifying the subsequent PSCAD/EMTDC results; they should not be interpreted as substitutes for the complete frequency-dependent and nonlinear EMT simulations.

For initial energization of an uncharged, lossless, open-ended transmission line, closing exactly at a source-voltage zero ideally produces no incident voltage wave. If the actual electrical making instant differs from the target by Δt, the approximate first receiving-end voltage factor is:

$$K\_first \approx 2|\sin(2\pi f \Delta t)|. \tag{43}$$

This expression represents an idealized first-arrival travelling-wave response. It does not include source impedance, line attenuation, interphase coupling, shunt compensation, pre-strike, or surge-arrester conduction, all of which are represented in the EMT model.

At 50 Hz, absolute timing errors of 0.50, 1.00, and 1.50 ms produce analytical first-arrival factors of 0.313, 0.618, and 0.908 pu, respectively. The nonlinear increase of K_first with timing error is illustrated in Fig. 2(a). Limiting the first-arrival factor to 0.50 pu requires:

$$|\Delta t| \leq 0.804\, ms, \tag{44}$$

10.48047/jocaaa.2026.35.08.03

whereas maintaining it below 1.00 pu requires:

$$|\Delta t| \leq 1.667\ ms. \tag{45}$$

These timing windows confirm that mechanical operating-time scatter cannot be neglected, even when the controller correctly identifies the voltage-zero target. In particular, the ±1.50-ms common operating-time limit adopted in the statistical framework can produce a substantial initial travelling-wave excitation unless it is compensated by the controlled-switching algorithm. For uncontrolled line closing with a uniformly distributed source-voltage angle θ, the idealized first-arrival factor becomes:

$$K\_first = 2|\sin(\theta)|. \tag{46}$$

The corresponding analytical mean, median, 98th percentile, and maximum are 1.273, 1.414, 1.999, and 2.000 pu, respectively. These quantities define the undamped open-end reference distribution and are not predictions of the final substation overvoltage. Differences between these values and the later EMT results must be physically attributable to the source strength, frequency-dependent line losses, compensation level, trapped voltage, pole coupling, or protective-device operation [6], [8], [9].

Transformer energization was examined using an analogous prospective-flux analysis. Neglecting the winding-resistance voltage drop during the first flux excursion, the normalized prospective peak core flux is expressed as:

$$\Phi\_peak \,/\, \Phi\_nom = 1 + |r + \cos(\theta)|, \tag{47}$$

where r is the residual flux normalized to the rated sinusoidal flux and θ is the actual electrical closing angle. The ideal residual-flux-matching condition is:

$$\cos(\theta *) = -r, \tag{48}$$

which limits the prospective peak flux to 1.0 pu when |r| ≤ 1. This relationship represents the theoretical basis of residual-flux-dependent transformer controlled switching [13]–[18]. The practical sensitivity analysis was conducted over the residual-flux interval:

$$-0.8 \leq r \leq 0.8\, pu. \tag{49}$$

With exact closing time but a residual-flux estimation error of up to ±0.10 pu, the worst prospective flux peak increases from 1.000 to 1.100 pu. A timing error of ±0.50 ms with exact residual-flux information results in a worst peak of 1.157 pu. When timing and residual-flux uncertainties are applied simultaneously, the calculated worst values increase to 1.257, 1.413, and 1.567 pu for timing-error bounds of ±0.50, ±1.00, and ±1.50 ms, respectively.

Figure 2(b) shows that the transformer-flux excursion increases monotonically as the electrical making-time error grows. The curve corresponding to a ±0.10-pu residual-flux estimation error remains above the exact-flux curve over the investigated range, demonstrating that timing

10.48047/jocaaa.2026.35.08.03

compensation alone cannot fully preserve the ideal energization condition when the magnetic state is estimated inaccurately. Nevertheless, even the combined ±1.50-ms and ±0.10-pu uncertainty case remains substantially below the analytical uncontrolled worst-case reference of 2.8 pu for $|r| \le 0.8$ pu.

Table 4. Analytical sensitivity of the controlled-switching targets

Equipment / Case	Condition	Calculated screening result
Line	Closing, timing error ±0.50 ms	K_first = 0.313 pu
Line	Closing, timing error ±1.00 ms	K_first = 0.618 pu
Line	Closing, timing error ±1.50 ms	K_first = 0.908 pu
Line	Maximum timing error for K_first ≤ 0.50 pu	0.804 ms
Line	Random closing, analytical U_2%	1.999 pu
Transformer	Ideal residual-flux matching	Φ_peak = 1.000 pu
Transformer	Residual-flux error ±0.10 pu	Φ_peak ≤ 1.100 pu
Transformer	±0.50-ms and ±0.10-pu errors	Φ_peak ≤ 1.257 pu
Transformer	±1.00-ms and ±0.10-pu errors	Φ_peak ≤ 1.413 pu
Transformer	±1.50-ms and ±0.10-pu errors	Φ_peak ≤ 1.567 pu
Transformer (Uncontrolled)	r ≤ 0.8 pu	Φ_peak ≤ 2.800 pu

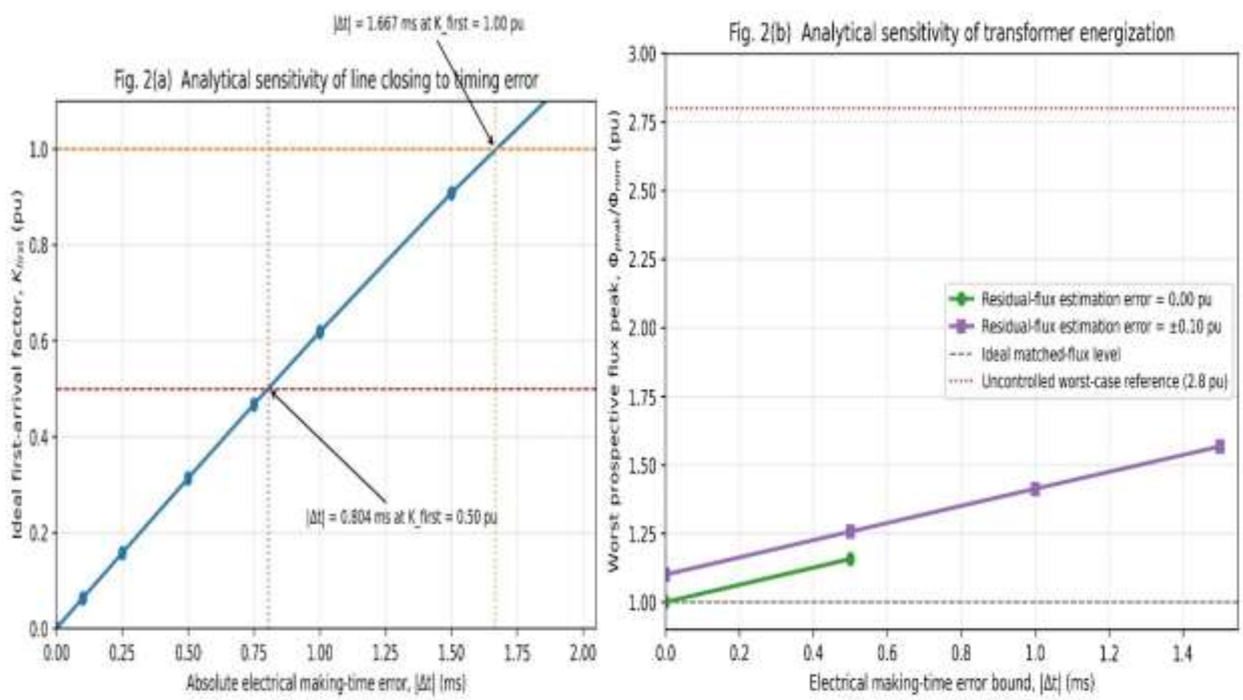

Fig. 2. Analytical sensitivity of the controlled-switching targets: (a) ideal first-arrival line-voltage factor as a function of electrical making-time error, and (b) worst prospective transformer-flux peak under timing and residual-flux estimation errors.

The curves in Fig. 2 are closed-form analytical screening results intended to clarify the sensitivity trends and establish verification expectations for the EMT simulations. The flux values quantify prospective magnetic excitation and must not be interpreted directly as inrush-current magnitudes, because the actual current also depends on the nonlinear saturation slope, three-phase core coupling, winding parameters, source impedance, and breaker-pole sequence. The subsequent EMT results should therefore reproduce the identified trends—progressive deterioration with

10.48047/jocaaa.2026.35.08.03

increasing timing and state-estimation errors—without being required to match the idealized numerical values exactly.

5.3. Probabilistic Analytical Screening under Practical Uncertainties

The combined effects of breaker operating-time scatter, pole dispersion, controller timing error, and transformer residual-flux estimation error were evaluated through a probabilistic analytical screening study. A total of 500,000 Monte Carlo operations were generated using the uncertainty distributions defined in Table 2 and a fixed random seed of 20260724 to ensure exact reproducibility. The common breaker-time error was shared by the three poles, whereas the pole-specific and controller errors were sampled independently. For the transformer cases, the residual-flux triplets satisfied

$$r_a + r_b + r_c = 0, \qquad (50)$$

with |r_k| ≤ 0.8 pu, while the residual-flux estimation error of each phase was uniformly distributed within ±0.10 pu.

For each line-switching operation, the maximum analytical first-arrival factor among the three phases was retained. In the controlled case, every pole targeted its corresponding source-voltage zero, and the actual making instant was displaced by the sampled timing error. In the uncontrolled case, a uniformly distributed common closing phase, the 120° phase displacement, and the same breaker uncertainties were applied. The resulting empirical cumulative distributions are shown in Fig. 3(a).

The controlled-switching distribution was shifted markedly toward lower values. Its mean and 98th-percentile first-arrival factors were 0.389 and 0.869 pu, respectively, compared with 1.907 and approximately 2.000 pu for uncontrolled closing. Thus, within the analytical screening model, controlled switching reduced the mean excitation factor by 79.6% and the 98th percentile by 56.5%. The probability of exceeding 1.0 pu decreased to 0.442%, and no realization exceeded 1.5 pu. These results indicate that the timing uncertainties adopted in Section 4 do not eliminate the benefit of voltage-zero targeting, although they produce a non-negligible upper tail that must be examined using the complete breaker pre-strike and RDDS model.

Transformer performance was evaluated using the maximum prospective flux peak among the three phases. For controlled switching, the closing target of each pole was calculated from its estimated residual flux, after which the sampled timing error was applied. The uncontrolled case used a common random closing phase with the corresponding phase displacements. As shown in Fig. 3(b), the controlled distribution remained concentrated near the rated flux level, whereas uncontrolled energization produced a substantially broader upper tail.

The mean prospective flux peak decreased from 2.042 pu under uncontrolled closing to 1.198 pu with controlled switching, corresponding to a reduction of 41.3%. The respective 98th-percentile values were 2.713 and 1.441 pu, yielding a 46.9% reduction. Only 0.637% of the controlled operations exceeded 1.5 pu, and none exceeded 2.0 pu in the 500,000 trials. By comparison, 89.96% of uncontrolled operations exceeded 1.5 pu, and 54.92% exceeded 2.0 pu.

10.48047/jocaaa.2026.35.08.03

Table 5. Probabilistic analytical screening results

[Note added in revision: Relative to uncontrolled switching the mean first-arrival factor is reduced by 79.6 % and the 98th-percentile value by 56.5 %. For the transformer the corresponding reductions are 41.3 % (mean) and 46.9 % (98th percentile).]

Equipment and strategy	Mean (pu)	Median (pu)	P95 (pu)	P98 (pu)	Maximum (pu)
Transmission line—controlled	0.389	0.357	0.764	0.869	1.281
Transmission line—uncontrolled	1.907	1.932	1.999	2.000	2.000
Transformer—controlled	1.198	1.182	1.386	1.441	1.697
Transformer—uncontrolled	2.042	2.058	2.643	2.713	2.800

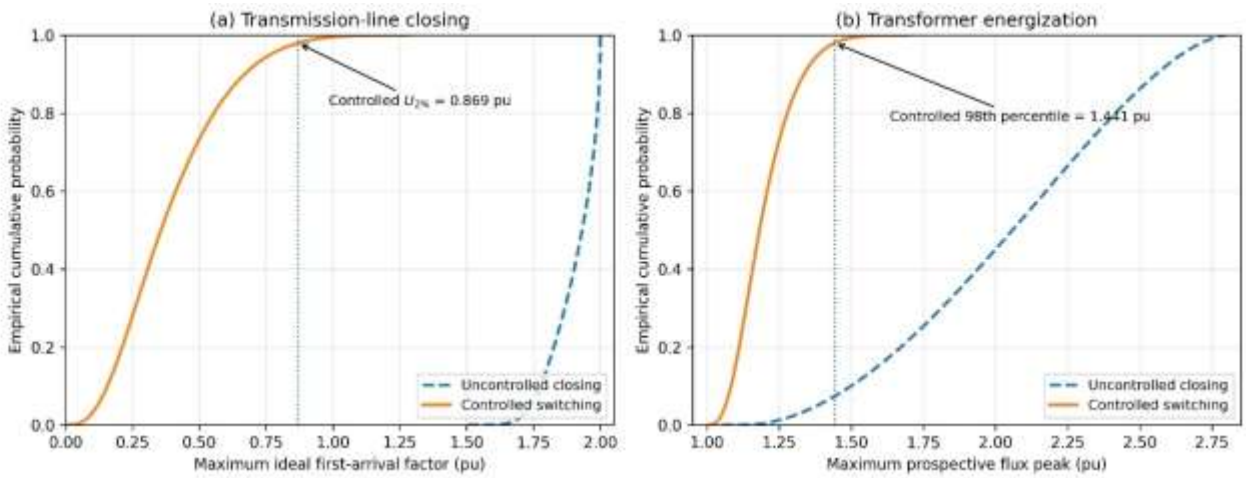

Fig. 3. Empirical cumulative distributions obtained from probabilistic analytical screening: (a) maximum ideal first-arrival line-voltage factor and (b) maximum prospective transformer-flux peak for controlled and uncontrolled switching.

The statistical separation observed in Fig. 3 supports the robustness of the proposed target-selection principles under the declared timing and state-estimation uncertainties. Nevertheless, these reductions must not be interpreted as the final performance of the 400-kV substation. The analytical line model excludes frequency-dependent attenuation, source-impedance interaction, trapped-charge dynamics, pre-strike, RDDS, and surge-arrester conduction. Likewise, the prospective-flux model does not calculate nonlinear magnetizing current or detailed three-dimensional core saturation. The final EMT simulations must therefore confirm the statistical ranking and qualitative trends rather than reproduce these screening values exactly.

5.4. Engineering Interpretation of the Analytical and Probabilistic Findings

The analytical and probabilistic results establish the operating conditions under which controlled switching can be expected to remain effective before the full EMT response is considered. For transmission-line energization, the first-arrival excitation is governed primarily by the error between the intended voltage-zero target and the actual electrical making instant. The deterministic screening showed that a 0.50-ms timing error produces an ideal first-arrival factor of 0.313 pu, whereas errors of 1.00 and 1.50 ms increase this factor to 0.618 and 0.908 pu. The probabilistic analysis subsequently confirmed that the combined common, pole-specific, and controller timing uncertainties produce a controlled 98th-percentile value of 0.869 pu, compared with approximately

10.48047/jocaaa.2026.35.08.03

2.000 pu for uncontrolled closing. This result demonstrates that voltage-zero targeting remains beneficial under the declared uncertainty model, but also shows that sub-millisecond prediction and compensation accuracy is required to suppress the upper tail effectively [3], [8], [9].

The transformer results lead to a complementary conclusion. Ideal residual-flux matching limits the prospective core-flux peak to 1.0 pu, while inaccuracies in both the estimated magnetic state and the breaker making time progressively weaken this condition. Under the combined statistical uncertainties, the controlled prospective-flux distribution retained a 98th-percentile value of 1.441 pu, substantially below the uncontrolled value of 2.713 pu. The finding confirms that accurate timing alone is insufficient: residual-flux estimation must also be included in the closing decision, particularly when the three core limbs retain unequal magnetic states [13]–[18].

The two sets of results further justify the coordinated formulation proposed in Section 3. A line-closing instant selected only to minimize the voltage across CB1 may leave an oscillatory or distorted receiving-bus voltage at the instant when CB2 is commanded. Conversely, delaying transformer energization solely to obtain a favorable flux-matching point may expose the line and arresters to a longer transient condition. The coordinated objective should therefore retain line overvoltage, transformer excitation, bus-voltage deviation, and arrester energy as simultaneous performance indices rather than optimizing either switching duty in isolation.

These screening results also define explicit acceptance expectations for the full EMT study. First, controlled switching should preserve a clear statistical separation from uncontrolled operation for both line overvoltage and transformer inrush current. Second, increasing breaker scatter, RDDS uncertainty, trapped-charge estimation error, or residual-flux error should degrade performance monotonically without reversing the overall method ranking. Third, the preferred strategy should remain effective across the specified ranges of line length, source short-circuit strength, compensation degree, and source X/R ratio. Finally, reductions in voltage or current must not be obtained at the expense of excessive arrester energy or violation of insulation-coordination limits [1], [2].

The numerical values reported in Sections 5.2 and 5.3 are therefore best interpreted as analytical performance bounds and verification targets. The final magnitude of the switching overvoltages and inrush currents must be determined from the complete frequency-dependent, nonlinear, and pre-strike-sensitive EMT model. Nevertheless, the present results provide a reproducible basis for identifying nonphysical simulations and for judging whether the subsequent EMT outcomes are consistent with the underlying switching and magnetic principles.

5.5. Evidence Status and EMT Acceptance Criteria

The findings reported in Sections 5.1–5.3 constitute analytical and probabilistic screening evidence rather than final EMT performance results. To maintain a clear distinction between these evidence levels, Table 6 identifies the claims currently supported and the corresponding confirmation required from the complete electromagnetic-transient model. Consequently, claims of quantitative overvoltage or inrush-current reduction on the complete 400-kV substation model must await the frequency-dependent, nonlinear EMT verification that is identified as the next required step.

Table 6. Evidence status and required EMT confirmation

10.48047/jocaaa.2026.35.08.03

Technical claim	Current supporting evidence	Required EMT confirmation
Voltage-difference targeting reduces line-closing excitation	Closed-form timing analysis and 500,000-trial analytical screening	Phase-to-ground and phase-to-phase overvoltages, U_2%, and exceedance probability
Residual-flux matching reduces transformer excitation	Prospective-flux analysis under timing and estimation errors	Nonlinear peak inrush current, core-flux trajectories, and bus-voltage deviation
Proposed switching outperforms alternative mitigation methods	Analytical comparison with uncontrolled switching	Paired comparison with uncontrolled switching, conventional controlled switching, surge arresters, and PIR
Performance is robust to practical uncertainty	Timing and residual-flux uncertainty screening	Sensitivity to line length, compensation, source strength, X/R, RDDS, and pre-strike
Mitigation is compatible with insulation and protection requirements	Analytical normalization and prescribed performance indices	Arrester energy, equipment-terminal voltages, and insulation-limit compliance

An EMT case is accepted only when the 5-μs solution differs by less than 1% from the 2.5-μs reference in maximum overvoltage, electrical making instant, peak inrush current, and arrester energy. Comparisons between mitigation methods must use paired random samples and identical physical initial states. The proposed method is considered robust only if its statistical ranking is preserved over the parameter ranges defined in (31)–(34), without transferring excessive duty to the surge arresters or producing unacceptable bus-voltage deviations.

5.6. Study Limitations

The reported numerical findings are analytical and probabilistic screening results intended to verify the physical consistency and uncertainty sensitivity of the proposed switching targets. They do not replace the final EMT evaluation of frequency-dependent line propagation, trapped-charge dynamics, breaker pre-strike and RDDS, surge-arrester conduction, transformer saturation, and three-phase magnetic coupling. Moreover, the baseline breaker distributions should be replaced by manufacturer or type-test data when the method is applied to a specific installation. The investigated system is a reproducible 400-kV benchmark rather than a confidential utility network; therefore, the sensitivity ranges are used to assess generality, while site-specific insulation levels, arrester capability, and operating constraints must be verified separately.

6. Conclusion

This study developed an integrated framework for analyzing and mitigating switching transients caused by transmission-line and power-transformer switching in a high-voltage substation. The framework combines a frequency-dependent line model, shunt compensation, nonlinear transformer representation, independently operated circuit-breaker poles, surge arresters, trapped voltage, residual flux, operating-time scatter, RDDS, and pre-strike within a coordinated switching formulation.

The proposed line-closing target minimizes the instantaneous voltage across each breaker pole, whereas transformer energization is based on matching the prospective and residual core fluxes. The command instants are corrected for mechanical delay and predicted pre-strike, and line and transformer switching are coordinated through overvoltage, inrush-current, bus-voltage, and arrester-energy indices.

10.48047/jocaaa.2026.35.08.03

Analytical verification established the electrical normalization bases and confirmed the expected line travelling time and line–reactor oscillation frequency. In the 500,000-trial probabilistic screening, controlled switching reduced the mean ideal line first-arrival factor from 1.907 to 0.389 pu and its 98th percentile from approximately 2.000 to 0.869 pu. The mean prospective transformer-flux peak decreased from 2.042 to 1.198 pu, while its 98th percentile decreased from 2.713 to 1.441 pu. These results indicate that the proposed targets remain effective under the declared timing and residual-flux uncertainties.

The complete EMT assessment must still confirm these rankings under frequency-dependent, nonlinear, and breaker-specific conditions rather than reproduce the idealized values exactly. Subject to that verification, coordinated controlled switching offers a technically credible means of reducing line overvoltages and transformer excitation without relying exclusively on pre-insertion resistors or surge arresters.

Data Availability Statement

The analytical screening results presented in this paper are fully reproducible from the closed-form expressions, the statistical distributions given in Table 2, and the fixed random seed 20260724. The underlying Monte-Carlo screening code will be made available by the corresponding author upon reasonable request. Detailed PSCAD/EMTDC case files for the complete frequency-dependent study will be released after the companion EMT verification paper is completed.

References:

[1] International Electrotechnical Commission, *IEC 60071-1:2019, Insulation Co-ordination—Part 1: Definitions, Principles and Rules*, 9th ed. Geneva, Switzerland: IEC, 2019.

[2] International Electrotechnical Commission, *IEC 60071-2:2023, Insulation Co-ordination—Part 2: Application Guidelines*. Geneva, Switzerland: IEC, 2023.

[3] CIGRE Working Group A3.35, *Guidelines and Best Practices for the Commissioning and Operation of Controlled Switching Projects*, CIGRE Technical Brochure 757. Paris, France: CIGRE, 2019.

[4] CIGRE Working Group C4.307, *Transformer Energization in Power Systems: A Study Guide*, CIGRE Technical Brochure 568. Paris, France: CIGRE, 2014.

[5] P. Mestas and M. C. Tavares, "Comparative analysis of techniques for control of switching overvoltages during transmission lines energization," *Electric Power Systems Research*, vol. 80, no. 1, pp. 115–120, Jan. 2010, doi: 10.1016/j.epsr.2009.08.011.

[6] K. M. C. Dantas, D. Fernandes Jr., W. L. A. Neves, B. A. Souza, and L. C. A. Fonseca, "Mitigation of switching overvoltages in transmission lines via controlled switching," in *Proc. 2008 IEEE Power and Energy Society General Meeting—Conversion and Delivery of Electrical Energy in the 21st Century*, Pittsburgh, PA, USA, 2008, pp. 1–8, doi: 10.1109/PES.2008.4596806.

[7] H. Seyedi and S. Tanhaeidilmaghani, "New controlled switching approach for limitation of transmission line switching overvoltages," *IET Generation, Transmission & Distribution*, vol. 7, no. 3, pp. 218–225, Mar. 2013, doi: 10.1049/iet-gtd.2012.0285.

[8] F. Deyhim and R. Ghanizdeh, "Insulation risk assessment of controlled switching considering pre-strike voltage and line trapped charge," *IET Science, Measurement & Technology*, vol. 13, no. 2, pp. 139–148, Mar. 2019, doi: 10.1049/iet-smt.2018.5150.

10.48047/jocaaa.2026.35.08.03

[9] F. Zhang, X. Duan, M. Liao, J. Zou, and Z. Liu, "Statistical analysis of switching overvoltages in UHV transmission lines with a controlled switching," *IET Generation, Transmission & Distribution*, vol. 13, no. 21, pp. 4998–5004, Nov. 2019, doi: 10.1049/iet-gtd.2019.1072.

[10] D. Barros, W. L. A. Neves, and K. M. C. Dantas, "Controlled switching of series compensated transmission lines: Challenges and solutions," *IEEE Transactions on Power Delivery*, vol. 35, no. 1, pp. 47–57, Feb. 2020, doi: 10.1109/TPWRD.2019.2916807.

[11] A. Karimonnafs, "Synchronous switching of uncompensated transmission line, by considering the effect of coupling voltage between the phases, trapped charge and the characteristics of CB," *IET Science, Measurement & Technology*, vol. 18, no. 1, pp. 12–24, Jan. 2024, doi: 10.1049/smt2.12164.

[12] M. Akafi-Mobarakeh, R. Shariatinasab, P. Siano, B. Vahidi, and H. R. Najafi, "A new model of trapped charge sources in switching transient studies in the presence of shunt reactors," *IEEE Access*, vol. 13, pp. 37118–37127, 2025, doi: 10.1109/ACCESS.2025.3544109.

[13] J. H. Brunke and K. J. Fröhlich, "Elimination of transformer inrush currents by controlled switching—Part I: Theoretical considerations," *IEEE Transactions on Power Delivery*, vol. 16, no. 2, pp. 276–280, Apr. 2001, doi: 10.1109/61.915495.

[14] J. H. Brunke and K. J. Fröhlich, "Elimination of transformer inrush currents by controlled switching—Part II: Application and performance considerations," *IEEE Transactions on Power Delivery*, vol. 16, no. 2, pp. 281–285, Apr. 2001, doi: 10.1109/61.915496.

[15] A. Ebner, M. Bosch, and R. Cortesi, "Controlled switching of transformers—Effects of closing time scatter and residual flux uncertainty," in *Proc. 43rd International Universities Power Engineering Conference*, Padua, Italy, 2008, pp. 1–5, doi: 10.1109/UPEC.2008.4651646.

[16] R. Cano-González, A. Bachiller-Soler, J. A. Rosendo-Macías, and G. Álvarez-Cordero, "Controlled switching strategies for transformer inrush current reduction: A comparative study," *Electric Power Systems Research*, vol. 145, pp. 12–18, Apr. 2017, doi: 10.1016/j.epsr.2016.11.018.

[17] J. Mitra, X. Xu, and M. Benidris, "Reduction of three-phase transformer inrush currents using controlled switching," *IEEE Transactions on Industry Applications*, vol. 56, no. 1, pp. 890–897, Jan./Feb. 2020, doi: 10.1109/TIA.2019.2955627.

[18] P. Pachore, Y. Gupta, S. Anand, S. Sarkar, P. Mathur, and P. K. Singh, "Flux error function based controlled switching method for minimizing inrush current in 3-phase transformer," *IEEE Transactions on Power Delivery*, vol. 36, no. 2, pp. 870–879, Apr. 2021, doi: 10.1109/TPWRD.2020.2995519.

[19] J. Ugarte-Valdivielso, J. I. Aizpurua, M. Barrenetxea, and B. G. Stewart, "Reinforcement learning-based controlled switching approach for inrush current minimization in power transformers," *Engineering Applications of Artificial Intelligence*, vol. 181, pt. 1, Art. no. 115288, 2026, doi: 10.1016/j.engappai.2026.115288.

[20] J. R. Martí, "Accurate modelling of frequency-dependent transmission lines in electromagnetic transient simulations," *IEEE Transactions on Power Apparatus and Systems*, vol. PAS-101, no. 1, pp. 147–157, Jan. 1982, doi: 10.1109/TPAS.1982.317332.

[21] N. Chiesa, B. A. Mork, and H. K. Høidalen, "Transformer model for inrush current calculations: Simulations, measurements and sensitivity analysis," *IEEE Transactions on Power Delivery*, vol. 25, no. 4, pp. 2599–2608, Oct. 2010, doi: 10.1109/TPWRD.2010.2045518.

[22] S. Jazebi, A. Rezaei-Zare, M. Lambert, S. E. Zirka, N. Chiesa, Y. I. Moroz, X. Chen, M. Martinez-Duro, C. M. Arturi, E. P. Dick, A. Narang, R. A. Walling, J. Mahseredjian, J. A. Martinez, and F. de León, "Duality-derived transformer models for low-frequency electromagnetic

10.48047/jocaaa.2026.35.08.03

transients—Part II: Complementary modeling guidelines," *IEEE Transactions on Power Delivery*, vol. 31, no. 5, pp. 2420–2430, Oct. 2016, doi: 10.1109/TPWRD.2016.2556686.

[23] IEEE Working Group 3.4.11, "Modeling of metal oxide surge arresters," *IEEE Transactions on Power Delivery*, vol. 7, no. 1, pp. 302–309, Jan. 1992, doi: 10.1109/61.108922.

[24] P. Pinceti and M. Giannettoni, "A simplified model for zinc oxide surge arresters," *IEEE Transactions on Power Delivery*, vol. 14, no. 2, pp. 393–398, Apr. 1999, doi: 10.1109/61.754079.

[25] International Electrotechnical Commission, *IEC 60099-4:2014, Surge Arresters—Part 4: Metal-Oxide Surge Arresters Without Gaps for A.C. Systems*, 3rd ed. Geneva, Switzerland: IEC, 2014.

[26] K. A. Bhatt and B. R. Bhalja, "An approach for controlled energization/re-energization of shunt compensated transmission lines," *International Journal of Electrical Power & Energy Systems*, vol. 120, Art. no. 105986, Sep. 2020, doi: 10.1016/j.ijepes.2020.105986.

[27] K. A. Bhatt, B. R. Bhalja, and U. B. Parikh, "Controlled switching technique for minimization of switching surge during energization of uncompensated and shunt compensated transmission lines for circuit breakers having pre-insertion resistors," *International Journal of Electrical Power & Energy Systems*, vol. 103, pp. 347–359, Dec. 2018, doi: 10.1016/j.ijepes.2018.06.024.

LEGEND OF REVISIONS (for Editor and Reviewers)

GREEN highlight: Major additions or structural corrections (completed equations, rewritten multi-objective coordination criterion, clarified evidence status and scope limitation of the present analytical/probabilistic screening, percentage-reduction note, Data Availability Statement).

YELLOW highlight: Minor language polishing, wording improvements and modest rephrasing of existing sentences for clarity and consistency with the revised scope statement.

All other text is retained from the original manuscript. Missing figures (Fig. 1–3) must still be supplied by the author as high-resolution images. The reference list has been kept complete as provided in the original submission.